

EXPERIMENTAL PROGRAM

Sample Preparation. The sample preparation consists of two stages. In the first stage, a deteriorated pavement slab is been extracted from the existing pavement and cut into a slab of dimensions 300 mm (length) \times 300 mm (width). The slab is placed in the bottom test box of the interface shear strength test apparatus and a tack coat is applied at the rate of 0.25 kg/sqm. as per MORTH specifications (MORTH, 2003) and allowed for emulsion breaking. After emulsion breaking time, the geosynthetic interlayers are placed as per experimental program before compacting the HMA overlay in the top box. The HMA mix is compacted into the top box of dimension 300 mm (length) \times 300 mm (width) up to a thickness of 50 mm.

Table 1. Physical properties of Tack coat

Properties	Values
Specific gravity	1.01
Penetration (1/10 th mm)	66
Brookfield Viscosity at 60 ^o C (centipoise)	460
Softening point (^o C)	52
Ductility (cm)	100+
Flash point and Fire point (^o C)	340, 365

Test Setup and Procedure. The Interface shear strength test setup consists of a large-scale shear strength apparatus having two shear boxes of size 300 mm (length) \times 300 mm (width) \times 100 mm (depth) separated by an interface zone. A detailed schematic of the test setup used in the current study is presented in Fig. 4. It can be observed that the test setup consists of two shear boxes with a movable bottom shear box and a fixed top shear box. These shear boxes are clamped together using shear clamps during the sample preparation process and removed prior to the commencement of the test. The tests are performed by applying constant vertical loads perpendicular to the specimen surface, with a constant shear displacement rate of 1 mm/min as per ASTM D5321 and UNI/TS 11214. A normal stress of 30 kPa, 60 kPa and 120 kPa are applied separately on the specimen interface combinations to determine the peak and residual shear characteristics. The specimen interface combinations consist of a no interlayer (control) case, followed by PE grid, PP grid and finally GJ mat placed at the interface of old and new pavement layers. The tests are performed for all the above interface conditions at different normal stress values applied and terminated once the shear displacement value reaches 50 mm.

RESULTS AND DISCUSSIONS

The peak and residual interface shear strength characteristics for all the interface conditions studied from the large scale interface shear strength tests were obtained separately from the shear stress and horizontal displacement output graphs. The output graphs are directly obtained from the software which gets the displacement and load values through data acquisition system.

The variation of shear stress with horizontal displacement for all the interface combinations tested in the current study is plotted as shown in Fig. 5. It is observed that the shear stress values are increasing with the increase in normal stress for all the interface conditions. The shear stress is observed to reach a peak value and then reduces to residual shear stress value under a large strain in all the samples tested. However, the peak interface shear strength between old and new pavement layers for control interface condition is witnessed to be more than all the

other interface conditions tested. The reduction in interface shear strength in case of interlayers is actually due to their own presence at the interface of old pavement layer (bottom layer) and the new HMA overlay (top layer). The interlayer provided at the interface creates a smooth surface, thus reducing the friction between layers and hence, a lower interface shear strength value is witnessed.

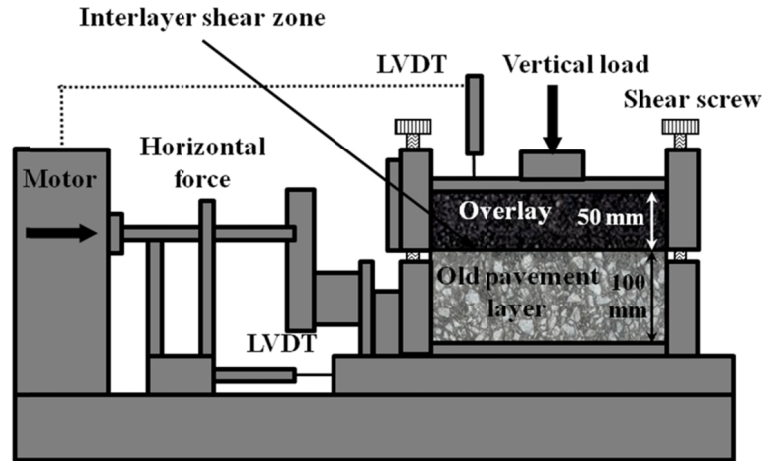


Figure 4. Schematic of Interface shear strength test setup.

The peak and residual state interface shear strength envelopes obtained for different interface conditions studied in the current research are presented in Figs. 6 and 7 respectively. The comparison of peak and residual state interface shear strength characteristics are presented in Table 2.

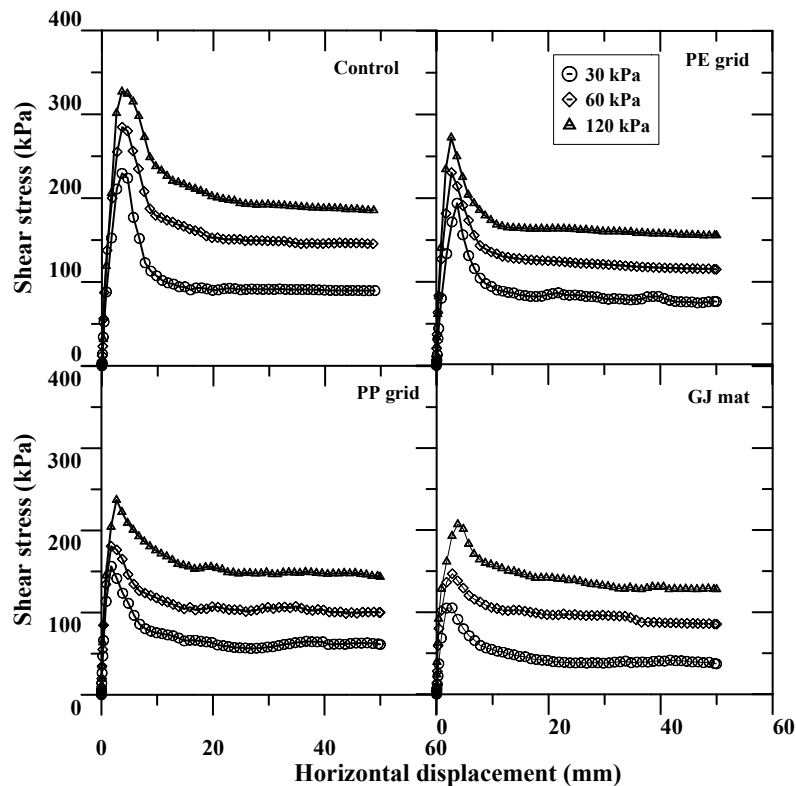


Figure 5. Variation of shear stress with horizontal displacement.

From Figure 6, it is evident that the interface shear strength between the old and new pavement layers is highest for control interface condition. Among the geosynthetic interlayered interface conditions, the higher interface shear strength is seen in the case of PE grid followed by PP grid and finally GJ mat with the least interface shear strength. The reason for this variation in interface shear strength would be due to the presence of apertures or mesh openings in case of PE grid and PP grids. The presence of apertures would help to improve the interface bond condition by a mechanism known as through-hole bonding (THB) action which is not witnessed in GJ mat, as there are no apertures. The above conditions were experienced by Canestrari et al. (2006) and Ferrotti et al. (2012) in their experimental studies. However, in contrary to their observations, the PP grid with a larger aperture (40 mm) opening compared to PE grid (18 mm) showed a lesser interface shear strength. The reason for reduced interface shear strength in case of PP grids would be due to their material composition, their thickness and their surface condition (smooth). The other reasons for higher interface shear strength in case of PE grid may due to the presence of polymer modified binder coating on PE grid, which enhances their bonding ability. The other reason would be the aperture size of PE grid which enables interlocking of the BC mix. It can be observed from Fig. 7 that, there is cohesion between the layers even at residual state. But, this condition is in contrast to the observations made by many researchers (Canestrari et al. 2006; Ferrotti et al. 2012), as they have assumed the cohesion at residual state to be equal to zero. However, there is a significant reduction in the friction angle from peak state to the residual state.

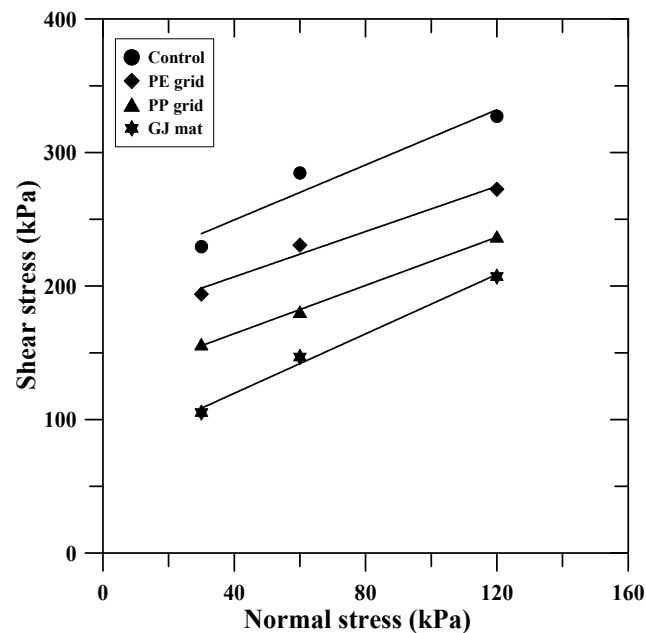


Figure 6. Peak state interface shear strength envelopes for different interface conditions.

From Figures 6, 7 and Table 2, it can be clearly distinguished that there is a reduction in the interface shear strength for the interface conditions with interlayers (either grid or textile) both at peak and residual states. To evaluate the reduction in interface shear strength, a performance factor known as the reduction in interface shear strength (RIS) is introduced. RIS can be mathematically expressed as:

$$RIS (\%) = \frac{IS_C - IS_I}{IS_C} \times 100 \quad (1)$$

Where, IS_C is the interface shear strength between old and new pavement layers for control interface condition, IS_I is the interface shear strength between old and new pavement layers for interlayered interface condition.

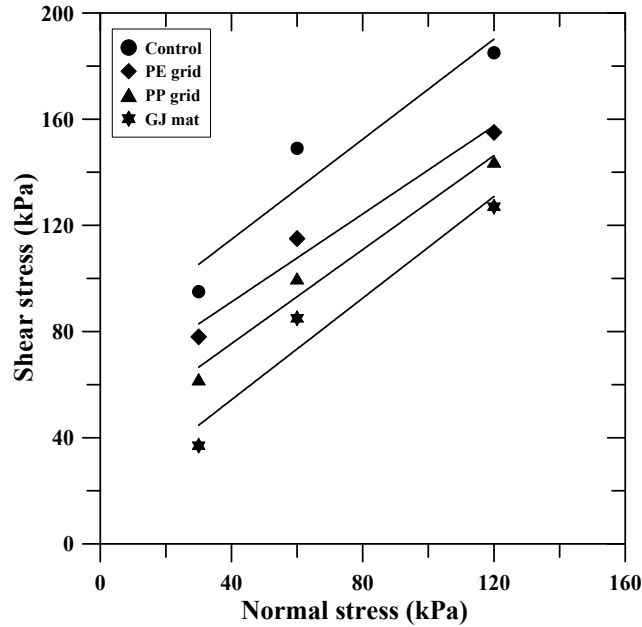


Figure 7. Residual state interface shear strength envelopes for different interface conditions.

Table 2: Peak and residual state interface shear properties

Interface condition	Peak state		Residual state	
	c (kPa)	Φ (deg)	c (kPa)	Φ (deg)
Control	208.26	45.87	77.05	43.31
PE grid	173.00	40.28	58.23	39.65
PP grid	128.18	42.09	40.10	41.53
GJ mat	75.10	48.07	16.71	43.74

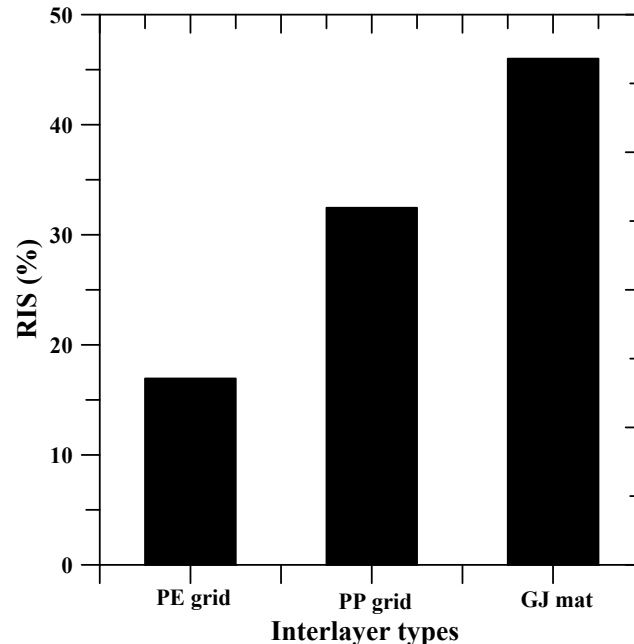


Figure 8. Variation of RIS (peak state) with interlayer types.

From Figure 8, it can be understood that GJ mat interface has the highest reduction in interface shear strength compared to the other interface conditions. The reason could be the absence of aperture openings in interlayer as there is no direct contact between the layers. The bonding between the old and new pavement layers is now completely dependent on the adhesion ability of an interlayer material (GJ mat) to the adjacent layers. The least reduction in interface shear strength is witnessed in the case of PE grid interface, although the aperture size of latter is lesser than PP grid interface. This simplifies the fact, that the interface shear strength is not only dependent on the aperture size of the interlayer placed at the interface. But, also depends on their material composition and their surface conditions (smooth or rough). The binder coating provided on the surface of PE grid help to enhance the interface shear strength by improving the adhesion property between the grid and surrounding (old and new) layers. Also, the presence of apertures further helps to enhance the interface shear strength value using THB mechanism.

CONCLUSION

The interfacial shear properties of geosynthetic interlayered asphalt overlays are determined using a large scale interface shear strength test and compared with the control interface condition in the current study. The following conclusions can be drawn from the study:

The interfacial bond strength for the control interface condition is witnessed to be consistently higher than the geosynthetic interlayered interface conditions. The reduced interfacial bond strength for the geosynthetic interlayered condition is due to the presence of geosynthetic interlayers, which creates a smooth interface reducing the friction between layers.

The interfacial bond strength for geosynthetic interlayered asphalt overlays was compared with that of control interface conditions and a performance factor, RIS was employed to study the reduction in interfacial shear strength of geosynthetic interlayered overlays. PE grid interface showed the least RIS with 17%, followed by PP grid with 32% and finally GJ mat with the highest RIS of 46%. The factors affecting the interfacial shear strength are the material composition, aperture openings and surface characteristics of the geosynthetic interlayer.

REFERENCES

- Al-Qadi, I. L., Fini, E. H., Elseifi, M. A., Masson, J. F., and McGhee, K. M. (2006). "Viscosity Determination of Hot-Poured Bituminous Sealants." *Journal of Transportation Research Board*, 1958, 74-81.
- ASTM D5321. Standard Test Method for Determining the Coefficient of Soil and Geosynthetic or Geosynthetic and Geosynthetic Friction by the Direct Shear Method, *Annual Book of ASTM Standards*, ASTM International, West Conshohocken, PA.
- Barraza, D. Z., Pérez, M. A. C., Fresno, D. C., and Zamanillo, A. V. (2010). "Evaluation of anti-reflective cracking systems using geosynthetics in the interlayer zone." *Geotextiles and Geomembranes*, 29(2), 130-136.
- Brown, E. R., Mallick, R. B., Haddock, J. E., and Bukowski, J. (1997). "Performance of Stone Matrix Asphalt Paving Mixtures (SMA) in the United States." *NCAT Report No. 97-01*, National Center for Asphalt Technology, Auburn, AL.
- Brown, S. F., Thom, N. H., and Sanders, P. J. (2001). "A study of grid reinforced asphalt to combat reflection cracking." *Journal Association of Asphalt Paving Technologists*, 70, 543-69.
- Caltabiano, M. A. (1990). *Reflection Cracking in Asphalt Overlays*. Thesis submitted to University of Nottingham for the degree of Master of Philosophy.
- Canestrari, F., Grilli, A., Santagata, F. A., Virgili, A. (2006). "Interlayer shear effect of geosynthetic reinforcements." *In: 10th International conference on asphalt pavements, Québec*.
- Carey, D. E. (1975). "Evaluation of Synthetic Fabrics for the Reduction of Reflective Cracking." *Louisiana Department of Highways, Report No. LA-70-1B (B)*.
- Cleveland, G. S., Button, J. W., and Lytton, R. L. (2002). "Geosynthetic in Flexible and Rigid Pavement Overlay." *Texas Transport Institute, Texas A&M University System, Report No. 1777-1*.
- Elseifi, M. A., and Al-Qadi, I. L. (2003). "A Simplified Overlay Design Model against Reflective Cracking Utilizing Service Life Prediction." *Journal of Transportation Research Board*, Paper No. 03-3285.
- Farshad, A. (2005). "Potential Applications of Paving Fabrics to Reduce Reflective Cracking." Jackson State University, Mississippi. *Federal Highway Report, FHWA/MS-DOT-RD-2005-174*.
- Ferrotti, G., Canestrari, F., Pasquini, E., and Virgili, A. (2012). "Experimental evaluation of the influence of surface coating on fiberglass geogrid performance in asphalt pavements." *Geotextiles and Geomembranes*, 34, 11-18.
- Ghauch, Z. G., and Abou-Jaoude, G. G. (2013). "Strain response of hot-mix asphalt overlays in jointed plain concrete pavements due to reflective cracking." *Computers and Structures*, 124, 38-46.
- Gransberg, D. D. (2006). "Correlating Chip Seal Performance and Construction Methods." *Transportation Research Board*.
- Khodaii, A., Fallah, S., and Nejad, F. M. (2009). "Effects of Geosynthetics on Reduction of Reflection Cracking in Asphalt Overlay." *Geotextiles and Geomembranes*, 27, 131-140.
- MORTH. (2003). Specifications for Road and Bridge Works, *Ministry of Road Transport and Highways, Indian Road Congress (IRC), New Delhi*.

- Prieto, J. N., Gallego, J., and Perez, I. (2007). "Application of the wheel reflective cracking test for assessing geosynthetics in anti-reflection pavement cracking systems." *Geosynthetics International*, 14(5), 287-297.
- Sanders, P. J., Brown, S. F. and Thom, N. H. (1999). "Reinforced Asphalt for Crack and Rut Control." *7th Conference on Asphalt Pavements*, Southern Africa.
- Sherman, G. (1982). "Minimizing Reflection Cracking of Pavement Overlays." *Technical Report, NCHRP Synthesis 92*.
- UNI/TS 11214. Mechanical Properties of Road and Airfield Pavements: Interlayer Shear Performance-related Characterization: *ASTRA Test Method*.

Sinkhole Early Detection System

Matthew A. Dettman, P.E.¹; and Ronald J. Rizzo²

¹Dept. of Engineering, Western Kentucky Univ., 1906 College Heights Blvd #21082, Bowling Green, KY 42101. E-mail: matthew.dettman@wku.edu

²Dept. of Engineering, Western Kentucky Univ., 1906 College Heights Blvd #21082, Bowling Green, KY 42101. E-mail: ron.rizzo@wku.edu

Abstract

A pilot study was performed to determine the viability of a permanently installed sinkhole detection device for use in both commercial and residential applications. The current state of the practice methods for sinkhole detection provide only a single snapshot in time of subsurface conditions. The theory investigated was the concept that if a sinkhole is forming underneath an existing structure, the void forming could be detected mechanically by a falling weight causing a trigger to alert occupants. The device would be installed through the existing floor and at a depth such that the sinkhole void could be detected prior to any damage to the structure. Prototypes were constructed and tested in various environmental conditions for durability and in simulated sinkhole conditions in the field. While impediments to widespread use exist, the device appears capable of serving as a sinkhole early detection system.

INTRODUCTION

Bowling Green, Kentucky is located on one of the most interesting sinkhole plains in the world and is the home of Mammoth Cave and the now famous National Corvette Museum (NCM) sinkhole collapse. Researchers at Western Kentucky University (WKU) in Bowling Green have been studying karst related geo-hazards for many years. After the February 11th, 2014 collapse at the NCM, research began under the auspices of the Engineering, Manufacturing, and Commercialization Center at WKU to develop methods of detecting and predicting sinkholes.

The current state of the practice methods for geophysical sinkhole detection include Microgravity Imaging (MI), seismic methods, Ground Penetrating Radar (GPR), and Electrical Resistivity Imaging (Burden 2012). All of these methods are capable of detecting Karst features, each having positive and negative characteristics. MI uses micro variations in the earth's gravity based on the density of subsurface materials to detect voids. While it can be very effective in detecting possible near-surface voids to improve locating invasive borings (Karem and Ealey, 2008) and can be used close to and inside structures, it can also be time consuming and expensive (Davis and Waters, 2015). Seismic methods are relatively inexpensive and are improving in effectiveness for sinkhole detection (Tran et al, 2013). However the accuracy can be somewhat unreliable (Sheehan et al, 2005). GPR methods are relatively inexpensive and effective in sands (Dobecki and Upchurch, 2006), however, use in clay soils is extremely limited (Doolittle et al, 2007). Although ERT may be emerging as the most effective method in most soil types and is improving in cost effectiveness due to wider use (Youssef et al, 2012), it has limitations in and around structures (Davis and Waters, 2015), (Dobecki and Upchurch, 2006)

The future of sinkhole detection and monitoring could be through interferometric synthetic aperture radar (InSAR). This method utilizes satellite-based radar (Kim and

Degradpre, 2016) or ground-based radar (Intrieri et al, 2015) to measure displacements in the ground surface which could be used to provide an early warning to an impending collapse. At this point, the method is very early in the research phase and cost prohibitive for practical use.

The common element that all of these methods share is that they all represent a single snapshot in time. It is well documented that sinkholes develop over long periods of time regardless of the specifics of the Karst environment (Beck and Sinclair, 1986), (Crawford, 1989). While an initial evaluation of a site is valuable on the front end of the design process, subsurface conditions in Karst environments can change dramatically over time. This concept, combined with the catastrophic events at the Corvette museum, led researchers at WKU to design, build, and test a permanently installed sinkhole monitoring system.

THEORY BEHIND PERMANENTLY INSTALLED MONITORING

One of the most common types of sinkholes is the cover-collapse sinkhole (Beck and Sinclair, 1986), (Crawford, 1989). In a cover-collapse sinkhole, solution cavities are formed in the underlying carbonate bedrock as a result of slightly acidic water percolating through the overburden soil and penetrating cracks and fissures of the limestone, causing it to slowly dissolve. As the void in the rock grows, the finest soil particles are carried downward into the void by the percolating groundwater creating a regolith arch (Crawford, 1989). The regolith arch is a high void ratio soil that is highly susceptible to collapse due to local instability or external influences such as vibrations. Over time, the regolith arch collapses starting at the bedrock level with the collapse moving slowly towards the ground surface, as illustrated in Figure 1.

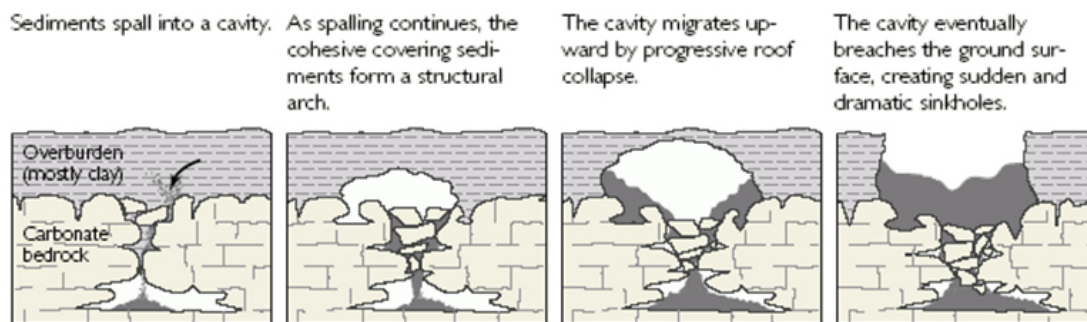


Figure 1 - Regolith Arch Collapse – From the USGS

As previously discussed, current Geophysical methods provide a view of the subsurface conditions at a single point in time. Once the subsurface investigation has been completed, and the site has been developed, the only way to determine if a cover-collapse sinkhole is developing is to repeat the Geophysical work repeatedly over the life of the development. The likelihood of even the most advanced subsurface investigations finding all possible voids and early stage regolith arch structures is virtually zero.

The permanently installed sinkhole detection device is one potential solution to this problem. The basic installed components of the device are shown in Figure 2.

The device is designed to be installed through a slab-on-grade and into the soil beneath an existing structure or in new construction. The depth of installation depends on the subsurface conditions and is generally assumed to be one-half the depth to bedrock. As this is a new device, there is no long term data to determine the optimal depth of installation. One-half the depth to bedrock is a “best estimate” based on the following 2 criteria; 1) Deep enough to detect the void

with enough advance notice for remediation measures, and 2) Not too deep to minimize installation costs and to not miss any voids that could be propagating laterally or in more of an inverted cone shape. The installation technique (described further below) is simply drilling a standard geotechnical type boring and inserting PVC pipe into the boring. This allows for the device to be installed at essentially any depth that can be achieved utilizing a standard geotechnical drill rig. Therefore, depths up to 100 feet are achievable, although it is anticipated that depths in the range of 20 feet to 50 feet would be more common.

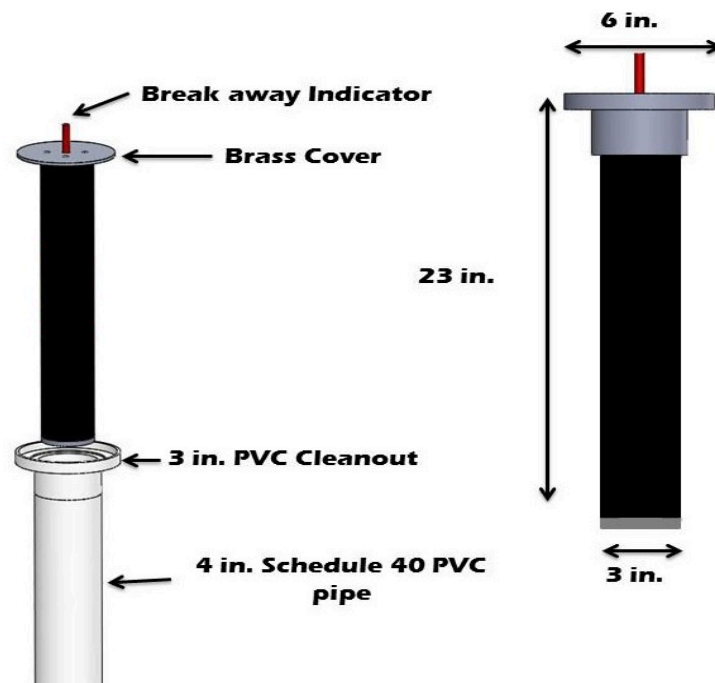


Figure 2 - Sinkhole Detection Device

The device is designed to trigger once a void is detected. The triggering mechanism is a falling weight which triggers a visible indicator at the top of the slab. Figure 3 shows the basic premise of the concept where a regolith arch collapse is rising to the surface, and the device is triggered prior to a collapse occurring that would adversely impact any structure at the ground surface. This could likely provide the time to perform the necessary stabilization before the loss of life or property occurs.

INSTALLATION METHOD

With the prototype device constructed, a method of installation was necessary and was developed through field testing. The design method of installation consisted of drilling a 5 inch boring to the desired depth and setting the 4 inch outer casing of the device into the boring. In practice, the top of the pipe would be flush with the finished floor elevation of the structure. The outer casing would then be filled with sand to within 23 inches of the top of the casing. The device, which is 23 inches long, would then be set into the outer casing and secured.

The purpose of the sand filled outer casing is to allow flexibility in the depth of the device without having to manufacture devices with different length. If a void propagates up to